Modeling and Optical Analysis of a Multilayer Surface Plasmon Resonance (SPR) Sensor Device Based on Silver, Tin Selenide, and Molybdenum Disulfide for Aqueous Media

Basaad Hadi Hamza, Sahar Abd Al-Aziz Mohammed, Fairooz Faeq Kareem, Farah Jawad Kadhum and Ali Abid Dawood Al-Zuky

College of Science, Mustansiriyah University, 10052 Baghdad, Iraq

bassaadhadi@uomustansiriyah.edu.iq, saharaziz1969@uomustansiriyah.edu.iq, Firooz.f @ec.edu.iq, farahjawadalnuaimi@uomustansiriyah.edu.iq, Prof.alialzuky@uomustansiriyah.edu.iq

Keywords: Surface Plasmon Resonance, Silver, Tin Selenide, Molybdenum Disulfide, Sensitivity, Biosensor.

Abstract: Surface plasmon excitation is dependent on the complicated refractive index of the metal, the thickness with optical characteristics of the metallic layer, and the angle of the incident light. MATLAB was employed to model the proposed multilayer system and to determine the conditions under which surface plasmon resonance (SPR) occurs, to evaluate its effectiveness as a sensor for detecting small variations or contaminations in the sensing medium. The proposed configuration consists of three layers: a thin tin selenide (SnSe) layer with a thickness ranging from 10 nm to 80 nm, a silver (Ag) layer with a fixed thickness of 50 nm, and a molybdenum disulfide (MoS_2) layer with a thickness varying from 10 nm to 80 nm in increments of 10 nm. The structure is deposited on a BK7-type glass prism using water as the sensing medium, where the refractive index variation (Δn) was considered of (0 and 0.01). Simulations were performed over a wavelength range of 100–1000 nm, in steps of 100 nm. To evaluate the surface plasmon resonance characteristics, reflectance (R) was plotted as a function of the incident angle (θ). The results improved SPR characteristics, including a sharper resonance dip, reduced full width at half maximum (FWHM), and enhanced resonance extent (Ld). The proposed SPR sensor achieved high sensitivity of 230°/RIU for $\Delta n = 0.01$ at $\lambda = 800$ nm, with $d(MoS_2) = 40$ nm and $d(SnSe) = 0$ nm, indicating strong performance in the infrared region. Additionally, variations in MoS_2 thickness exhibited a slight influence on the resonance angle due to the refractive index of the sensing medium. The observed shift in the R–θ curve demonstrates the great stability and sensitivity of the developed SPR sensor in the near-infrared spectral range, confirming its capacity to detect minor changes in refractive index in aqueous environments.

1 INTRODUCTION

Sensors which depends on surface plasmon resonance (SPR) limit molecular binding disturbance and eliminate time-consuming labeling processes, that's why it's considered they are the most favorable sensors for high-speed and high-sensitivity bio-molecular detection [1]. They have contributed significantly to the sensing and monitoring of a variety of biomolecular interactions, including DNA hybridization and protein binds [2]. A diagrammatic representation of the propagation of an electron density wave or plasma oscillation is formed at the metal-dielectric interface in the case of surface plasmon wave (SPW) biosensors. The resonant frequency of the SPW is simulated by incident light. In other words, resonance happens at the surface when light beams strike the contact and align with the surface plasmon (SP) wave vector [3].

The most popular process for exciting SPs is prism combination. Two configurations, the Otto and Kretschmann's–Raether configuration, can be used to achieve prism coupling [4], [5]. Attenuated entire internal reflection serves as the foundation for both setups. The most popular arrangement for SPR method observation is Kretschmann's. In conventional SPR sensor configuration, a thin metallic layer (composed of silver or gold) is placed between the sensing medium and prism. This layer facilitates SP propagation [6]. In this study, the reflected angle variation aids in identifying the type

of biological material that must be maintained on the biosensor.

SPR serves as a precise method for detecting alterations in refractive index close to a metal surface, rendering it a potent tool in the fields of biology and chemistry. Traditional SPR systems utilize a semicircular prism (like a Kretschmann prism) to couple light to surface plasmons at a designated angle. This configuration enables the resonance condition to be met with high efficiency while avoiding direct light absorption. Applications such as diagnosing diseases, monitoring biological reactions in real time, and identifying toxins or pollutants utilize this technology.

However, this kind of biosensor would have trouble tracing far-off and remote species. Furthermore, only this kind of SPR-based biosensor is suitable for huge systems with expensive projects. Consequently, it would only be appropriate to work in a laboratory [7].

Numerous scholars and researchers have examined the system of SPR sensor and have endeavored to develop to these systems that function as sensors to identify any alterations in the optical characteristics of the media being examined. One of the studies, for instance, is M. Saifur Rahman et al. (2017) [8]: explains the performance design of two different kinds of biosensors coated with graphene. The suggested SPR biosensors are analyzed using the angular examination method to establish resonance conditions. The sensitivity attributes of the proposed graphene-coated SPR biosensor in prism are investigated and contrasted with those of a conventional SPR sensor that lacks graphene.

Nisha et al. (2019) [9] they deposited a layer of MoS2 sandwich through the (Au and Ni) films. They exposed that addition graphene to the Ni film increased its sensitivity to 229°/RIU. They also found that the recommended sensor's sensitivity changes as the number of graphene and MoS2 layers grows. An SPR sensor with a hybrid structure comprising metal layers (Au, Ag, or Cu) and flattened materials (graphene, MoS2, WS2, and WSe2) is shown by Lin et al. (2020) [10] in order to use genetic algorithms to maximize sensitivity for a specific incident light wavelength. They found that the proposed sensor with an Ag layer have improved numerically sensitive of the 194°/RIU and varied substantially with incident ray wavelength related to Au (159°/RIU) and Cu (155°/RIU) using water as a detecting intermediate.

A bimetallic SPR sensor was simulated by Kadhum, F.J. et al. (2021) [11] by mimicking the titanium oxide (TiO2) (dTiO2=50nm) and silver (dAg =10-80nm) layers that were positioned on the semicircular glass prism D-ZLAF50. Characteristics of SPR angle (θSPR) are identified; SPR is notably observed at (600-700) nm from the range of the visible spectrum and (900-1000) nm of the infrared range. This sensor can be employed in these areas at (S=140°/RIU), as observed in the visible spectrum where the SPR dip extent (Ld) and full width half maximum (FWHM) values are ideal for silver layer thicknesses of 40–60 nm.

Kadhum, F.J. et al. (2021) [12] conducted an SPR simulation study where they coated a glass prism of type D-ZLAF50_Thick lanthanum flint with a gold (Au) layer 40 nm in thickness and polyvinyl alcohol (PVA) polymer layers of varying thicknesses. Several wavelengths were used for the analysis, ranging from (100 -1000) nm i.e. form UV to near-infrared. The greatest sensitivity of 207.5 °/RIU was achieved for PVA thicknesses of (30- 40) nm; changes in the sensitive medium refractive index (0, 0.04, 0.08, and 0.12) were successfully detected. Tin selenide (SnSe) and graphene are employed in a fresh surface plasmon resonance-based optical biosensor design by Ahmad M. Alsaad and colleagues (2023) [13]. They demonstrated that the suggested sensor can detect breast cancerous cells, skin, cervical, blood, and adrenal glands with sensitivity of 121.0 °/RIU, 134.2 °/RIU, 142.9 °/RIU, and 143.6 °/RIU, respectively, with a quality factor of maximum value 408 °/RIU.

Baidaa K. Hamed et al. (2025) [14], they developed simulation model using Matlab with variable of limitations within a wavelength band ranging from UV band to near IR band, the action of the plasmonic variation in gold(Au) thickness, (SnSe) tin selenide is measured at these bands. The SPR for gold coating having fixed thickness of (50 nm) and variable thickness (10-80 nm) of SnSe coating using glass prism type BK7_ glass with water as sensitive medium and refractive index (Δn = 0 and 0.01). The sensitivity (S) of SPR about (240°/RIU) at dSnSe equal to 80nm, (Ld.=0.947o) and (FWHM=5.6o).

This study aims to utilize appropriate computational methods to develop an SPR biosensor with high sensitivity. A certain formation of the Ag/SnSe/MoS2 metal has played a significant role in modeling of the refractive index bio-sensor features within the proposed innovative structure. In the current study, a simulation technique that used Fresnel equations and (TMM) method to calculate electromagnetic waves' reflectance between 100 and 1000 nm.

2 THEORETICAL MODELING OF SPR BIOSENSOR

SPR denotes the oscillation at resonance of free electrons on the surfaces of metal as a result of their interaction with incoming light. This phenomenon represents a specialized type of SPR, usually seen in nanoscale metal particles like gold, silver, and copper. Resonance occurs when the free electrons' natural oscillation frequency coincides with that of the incoming light [15].

When light strikes a thin metal sheet at a particular angle of incidence, the electrons in the sheet become excited and move in tandem with the sheet; this phenomenon is known as SPR. The angle of incidence that induces SPR is correlated with the material's refractive index. Therefore, if there is even a slight alteration in this index, it will impede SPR detection, assuming the wavelength of the light source and the thickness of the metal sheet are unchanged. Consequently, SPR can identify specific compounds or analytes, resulting in the creation of SPR biosensors aimed at detecting various significant biomarkers [16]. A non-radiative electromagnetic surface wave known as surface plasmon polarization travels along the interface between the dielectric material and negative permittivity. These oscillations are particularly sensitive to alterations in this boundary such as the adsorption of molecules on the conductive surface because of the wave that resides at the interface between conductor and external medium (like air, water, or vacuum) [17]. Localized surface plasmon resonances (LSPRs) refer to the collective oscillations of electron charge in metallic nanoparticles that are excited by light. There is a considerable increase in the near-field amplitude at the resonance wavelength. While resonance boosts far-field scattering from the nanoparticle, this effect is confined to a small area close to the nanoparticle surface and diminishes quickly with distance into the surrounding dielectric medium. Enhancement in light intensity is a crucial component of LSPRs, and localization allows for extremely high spatial precision (sub-wavelength) that is only constrained by nanoparticle size. The magneto-optical effect and other amplitude-dependent phenomena are additionally amplified by LSPRs due to the increased field amplitude [18], [19]. Surface plasmon polarizations can be excited resonantly through electron bombardment or by incident light beams, usually within the visible or infrared spectrum. For resonance to occur, the momentum of the incoming beam must align with that of the surface plasmon [20]. Resonance takes place when the electric field is aligned with the plane of incidence, which involves p-polarized light. It is possible to fulfill this condition by transmitting light through a medium with a high refractive index, like a glass prism. This raises the in-plane wavevector (momentum) and allows for resonance at a particular angle and wavelength. On the other hand, s-polarized light, which has its electric field oriented perpendicular to the plane of incidence, cannot generate surface plasmons because there is no suitable component of the electric field along the interface.

Even if both media are transparent, the electromagnetic wave disperses at the boundary when the photon beam strikes the material. The percentage of incoming electromagnetic waves that are reflected at the interface is known as reflectivity (R), and it is defined as follows [21].

$$R = \frac{I_r}{I_0} = \left(\frac{(n-n\_i)}{(n+n\_i)}\right)^2 \quad (1)$$

Where I_0 is the intensity of incident beam and I_r is the intensity of reflected beam, while n & n_i are the reflective indices for first and second medium, respectively.

This study demonstrates a simulation process to analyze SPR for different conditions. The simulation model for the multilayer SPR system was created using the transfer matrix method (TMM). Computed the reflection of electromagnetic waves in the visual and near-infrared regions using the Fresnel equations and suitable boundary conditions. The total characteristic matrix was utilized to link the electric and magnetic field amplitudes at the first interface ($E_\propto$ & $B_\propto$) with those at the final interface (EN & BN) in the N-layer model in order to calculate the reflectance of the multilayer structure deposited on the substrate [22].

$$\begin{bmatrix} E_\propto \\ \mathrm{B}_\propto \end{bmatrix} = \left[\prod_{i=1}^{N} M_i\right] \begin{bmatrix} E_\propto \\ B_\propto \end{bmatrix} = \begin{bmatrix} m_{11} & m_{12} \\ m_{21} & m_{22} \end{bmatrix} \begin{bmatrix} E_\propto \\ B_\propto \end{bmatrix}. \quad (2)$$

The real transfer matrix M_i of the i-th layer (I = 1 to N). It is organized in order between a prism and a sensing layer, which is calculated using the following relation.

$$M_i = \begin{bmatrix} cos\delta_i & \frac{isin\delta_i}{\delta_i} \\ iy_i sin\delta_i & cos\delta_i \end{bmatrix}. \quad (3)$$

In this instance δ_i is the optical phase addition resulting from a single field traversing the layer and can be written as.

$$\delta_i = \left(\frac{2\pi}{\lambda}\right) n_i d_i cos\theta_i. \quad (4)$$

The i-th layer's angle of incidence is (θ_i), n_i denotes the refractive index, d_i indicates the thickness, λ signifies the wavelength of light that strikes a vacuum. Below is the parameter for each layer γi in p-polarization [23].

$$\gamma_i = \frac{n_i\sqrt{\varepsilon_0\mu_0}}{cos\theta_i}. \quad (5)$$

Where ε_0 is the vacuum permittivity and μ_0 denotes the permeability. Surface plasmons that are electronic and magnetic follow this dispersion relation.

$$K(\omega) = \frac{\omega}{c}\sqrt{\frac{\varepsilon 1\varepsilon 2\mu 1\mu 2}{\varepsilon 1\mu 1+\varepsilon 2\mu 2}}. \quad (6)$$

Where (ω) denotes the angular frequency, (c) represents the speed of light in a vacuum, K (ω) is the wave vector, (ε) indicates the relative permittivity, and (μ) refers to the relative permeability of the material (1: the block, 2: the metal film) [22].

By figuring out the optical characteristics of the system, the optical appearances of the suggested SPR sensor were assessed in this work. A computer and spectrometer collect data when a light source emits light with a specific wavelength. Prism-based SPR biosensors work by reflecting light. This simulation computes the reflectance of films as long as the thickness of the film is similar to the wavelength of the incident light. Through the use of the simulation program, the details of the layer above the prism, the thickness of the metal thin-film in the prism, the type of dielectric, and the incident radiation (the wavelength of the incoming light), the recital factors of a sensor as functions of the silver substance have been effectively optimized. This work demonstrates how to investigate SPR for various boundaries through simulation techniques. The values for transmission (t) and reflection (r) between the layers can be calculated with the formula provided relation below [23].

$$r = \frac{\gamma_N m_{11}+\gamma_0\gamma_N m_{12}-m_{21}-\gamma_0 m_{22}}{\gamma_N m_{11}+\gamma_0\gamma_N m_{12}+m_{21}+\gamma_0 m_{22}}, \quad (7)$$

$$t = \frac{2\gamma_0(\frac{n_N}{n_0})}{\gamma_N m_{11}+\gamma_0\gamma_N m_{12}+m_{21}+\gamma_0 m_{22}}. \quad (8)$$

These equations can be used to examine the rearrangement of incident light energy and compute the reflective light, $R = |r|^2$ of a stack with multiple layers. SPR waves are produced as a result of this redistribution and depend on the reflected field power and incidence angle. Equation (3) can also be used to estimate the transmission $T = |t|^2$ over the stack multilayer.

Metrics like extent dip (Ld), full-width half maximum (FWHM), and sensitivity (S) can be used to analyze a sensor's performance. Sensitivity can be described as the ratio of the change in SPR angle (ΔθSPR) to the change in RI of the recognized medium (Δn), expressed as relation. [23].

$$S = \frac{\Delta\theta_{SPR}}{\Delta n}\ (°/\text{RIU})\ . \quad (9)$$

The algorithm can be said to primarily depend on the Fresnel equations and the transition matrix when the angle of incidence of light and the refractive indices of the various media in the plasmonic resonance system are known, with these indices typically remaining constant for each wavelength. The only medium that has a variable refractive index is the sensing medium where contamination is to be identified. The subsequent content is condensed and arranged as described above.

2 PROPOSED SPR SENSOR STRUCTURE

The outputs of the aforementioned equations can be utilized to determine FWHM, extent dip (Ld), and sensitivity, among other criteria, to quantify and assess the system's efficiency. For this work, the reflectance of P-polarized electromagnetic wavelengths P (λ) in the 100 nm to 1000 nm range of Fresnel equations was selected, and a simulation program was developed using Matlab_2018 b tools for a system of the following: A Prism: consist of a half-sphere of glass BK7 manufacture. Silver layer: made up of silver (Ag) film with thickness (50) nm. Tuning layer: created by combining MoS2 with a thickness of 40 nm and a SnSe film with thicknesses that vary (10-80) nm it's considered as Spectral Response Modulation Layer and the function of SnSe is to modify the resonance angle. The sensing medium: water (H_2O) is used because it's a good sensitive media. Refractive indices: water indices, n (λ), will be different by the amount (Δn = 0) in the case of no water pollution and (Δn = 0.01) in the case of water pollution. The wavelength: changes from (λ=100-1000) nm.

Three layers were deposited with transfer matrix using of an optical system that included a hemispherical prism, namely the BK7 glass half sphere prism: a thin layer of tin selenide (SnSe) having thickness ranging from (10 – 80) nm, and a second layer of silver (Ag), with a thickness of 50 nm, while the third layer thickness of the MoS2 layer from (10 - 80) nm in increments of 10. Water, a medium

used for chemical or biological sensitivity, serves as the sensitive medium in this investigation. The graphic drawing of the suggested SPR sensor is shown in Figure 1.

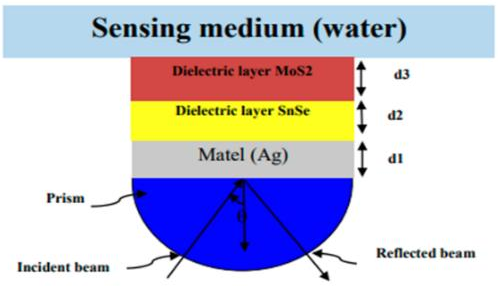

Figure 1: The representation illustration of surface Plasmon resonance sensors arrangement.

3 RESULTS AND DISCUSSIONS

This work represents the first phase of the study, focusing on improving the thickness of the MoS_2 layer. The study will later be expanded to include multi-layer and hybrid structures. To assess the performance of the suggested Ag/SnSe/MoS_2-based multilayer structure, its refractive index sensing characteristics were modeled. Because of its high sensitivity, the sensor can be used in both the visible and infrared portions of the electromagnetic spectrum. The sensitivity of the sensor was evaluated by analyzing reflectance curves as a function of the incidence angle. In order to identify the configuration that produces the highest sensitivity, simulation results were produced for a range of SnSe layer thicknesses (0, 10, ..., 80 nm). The SnSe layer in the suggested sensor design varied in thickness from 0 to 80 nm, while the silver (Ag) layer was fixed at 50 nm. For baseline assessment, the MoS_2 layer was first set at 40 nm. The goal of this simulation is to identify the ideal locations for plasmonic resonance, which has not been accomplished in previous studies employing this model. Our work aims to provide a suitable design and numerical values for the characteristics that might aid in enhancing the usefulness of optical sensors, while earlier research focused on different materials and methodologies. This summary will focus on the significance and creativity of the current work while offering more precise insights into the advantages and potential real-world applications. The numerical results of Ag, SnSe and MoS2 films lists in Table 1, were used to simulate the SPR within a small range according to the prism diagram. It illustrates how θSPR varied with MoS2's refractive index (Δn) at various wavelengths and layer thicknesses. Due to its sensitivity to both visible and infrared range, the introduced system operated with, which provides it an extensive variety of applications. FWHM, extent dip (Ld), and (S) values were obtained with a change in the refractive index (Δn) and can be change as (dSnSe = 0 - 80) nm with increments of unit 10 of the curve of (R–θ) analysis data. The results show that FWHM changed with the layer thickness. Figure 2 illustrates the reflectance curves in relation to varying light incident angles (R-θ curve) for diverse SnSe layer sheet thicknesses and wavelengths (λ) fluctuating from (100 to 1000) nm, with a unit step of 100 nm. This graphic demonstrates the SPR not appeared at 700 nm. The sensor layer absorbs the energy of SPR waves, resulting in low reflectance at the Ag/SnSe/MoS2 interface across all angles, also the SPR began at wavelength (710,730,750,770,790 and 800) nm. It is clear that a change in the refractive index causes a shift in the SPR dips in the visible and infrared regions, which significantly affects how well SPR sensors work. The dip's measurements, including its breadth and height, are also crucial. Strong appearance in (θSPR =85^o -72^o) fluctuating to slight angle with increased of wavelength range and increased of thicknesses with Δn = (0 to 0.01) for infrared region (710 nm to 800 nm) at dSnSe equal to (0-80) nm increments 10 nm step. From figure (2) noticed that Δn, it is the degree of variation in the sensing medium's refractive index, which is water. That is, its value represents the amount of contamination that causes a change in the value of the refractive index of water, not the semiconductor layer.

The computed Full-Width Half Maximum (FWHM) and the dip extent (Ld) as a function of dSnSe for both Δn values for several (λ) are illustrated in Figure 3. The finest results at λ (700,810, 910 and 1000) nm. It is noted that: When dSnSe = (0, 10……. 80nm): at dSnSe = 0 nm, the FWHM for the SPR dip is (3^o -4.8^o) at infrared region λ= (790-800) nm, increasing with increased of Δn and wavelengths. dSnSe =10 nm, the FWHM for the SPR dip is (1.2^o -1.4^o) at λ= (790-800) nm, increasing with increased of Δn and wavelengths. When dSnSe =20 nm, the FWHM for the SPR dip is (0.7^o -1^o) at infrared region λ= (790-800) nm, increasing with increased of Δn and wavelengths. While dSnSe=30 nm, the FWHM for the SPR dip is (0.6^o -0.7^o) at infrared region λ= (790-800) nm, increasing with increased of Δn and wavelengths. At dSnSe=40 nm, the FWHM for the SPR dip is (0.6^o -1.5^o) at infrared region λ= (790-800) nm, increasing with increased of Δn and wavelengths. And when dSnSe= (50-60) nm,

no SPR appear. At dSnSe=70 nm and λ= (710-770) nm, the FWHM for the SPR dip is (2.4° -2.6°) at infrared region, increased with an enlarged Δn , and reduced with increased wavelengths (0.6° – 10.5°). And dSnSe=80 nm, the FWHM for the SPR dip is (5.1° -5.4°) at infrared region λ= (710-800) nm, increased with an enlarged Δn and reduced with increased wavelengths (0.7° – 1.8°). Similarly noticed that the SPR dip extent (Ld) approximately -stable at all Δn values, at IR region bands λ= (790-800) nm: When d_{SnSe}=0 nm, the Ld for the SPR dip is (0.92° - 0.92°) stable with an increased Δn, and wavelengths. While dSnSe= 10 nm, the Ld for the SPR dip is (0.85° -0.93°) increased with an increase of Δn with wavelengths. At dSnSe= 20 nm, the Ld for the SPR dip is (0.67° -0.69°) increased with an increased Δn and wavelengths. dSnSe= 30 nm, the Ld for the SPR dip is (0.53° -1°) increased with an increased Δn , and wavelengths. At dSnSe= 40 nm, the Ld for the SPR dip is (0.53° -0.46°) decreased with an increase of Δn, and wavelengths. When dSnSe = (50-60) nm, no SPR appear. While when dSnSe=70 nm at λ= (710-770) nm, the Ld for the SPR dip is (0.36° -0.29°) decreased with an increased Δn, and wavelengths. At dSnSe=80 nm at λ= (710-800) nm, the Ld for the SPR dip is (0.45° -0.09°) decreased with an increased Δn, and wavelengths. The reflectance–angle simulations show that the SPR dip vanishes at SnSe thicknesses of 50 nm and 60 nm. This phenomenon is due to a mismatch in optical phase conditions and weakened coupling between the incident p-polarized light and the surface plasmon wave vector or propagation constant (SPW) at the metal–dielectric interface. The increase in thickness of the SnSe layer results in a greater phase delay and changes the effective optical path length, impacting the phase-matching condition required for the excitation of surface plasmons. Destructive interference can occur between incident and reflected light waves at certain thicknesses (especially 50–60 nm), which hampers energy transfer to surface plasmons and suppresses resonance.

Table 1: SPR dips, as a function of refractive index (Δn) varies with dSnSe from 0 to 80 nm in 10-unit increases.

d_{SnSe} nm	Δn	θ_{SPR} at λ 710	θ_{SPR} at λ 730	θ_{SPR} at λ 750	θ_{SPR} at λ 770	θ_{SPR} at λ 790	θ_{SPR} at λ 800
d_{SnSe} = 0	0	-----	-----	-----	------	79.5	83.0
	0.01	------	------	------	------	81.5	84.5
d_{SnSe} = 10	0	70.0	------	-------	------	74.5	76.0
	0.01	71.5	-------	------	------	76.5	77.5
d_{SnSe}=20	0	70.0	-------	-------	------	72.5	73.0
	0.01	72.0	-----	------	------	74.0	74.5
d_{SnSe}=30	0	------	71.5	------	------	71.5	72.0
	0.01	------	72.0	-------	-------	73.0	73.5
d_{SnSe} =40	0	------	--------	71.0	------	71.0	71.0
	0.01	------	-------	72.0	-----	72.5	72.5
d_{SnSe} =70	0	72.0	71.0	------	70.5	------	-----
	0.01	73.0	73.5	-------	72.5	------	-----
d_{SnSe} =80	0	72.5	71.5	73.0	------	-------	70.5
	0.01	74.0	73.5	74.5	------	72.0	72.0

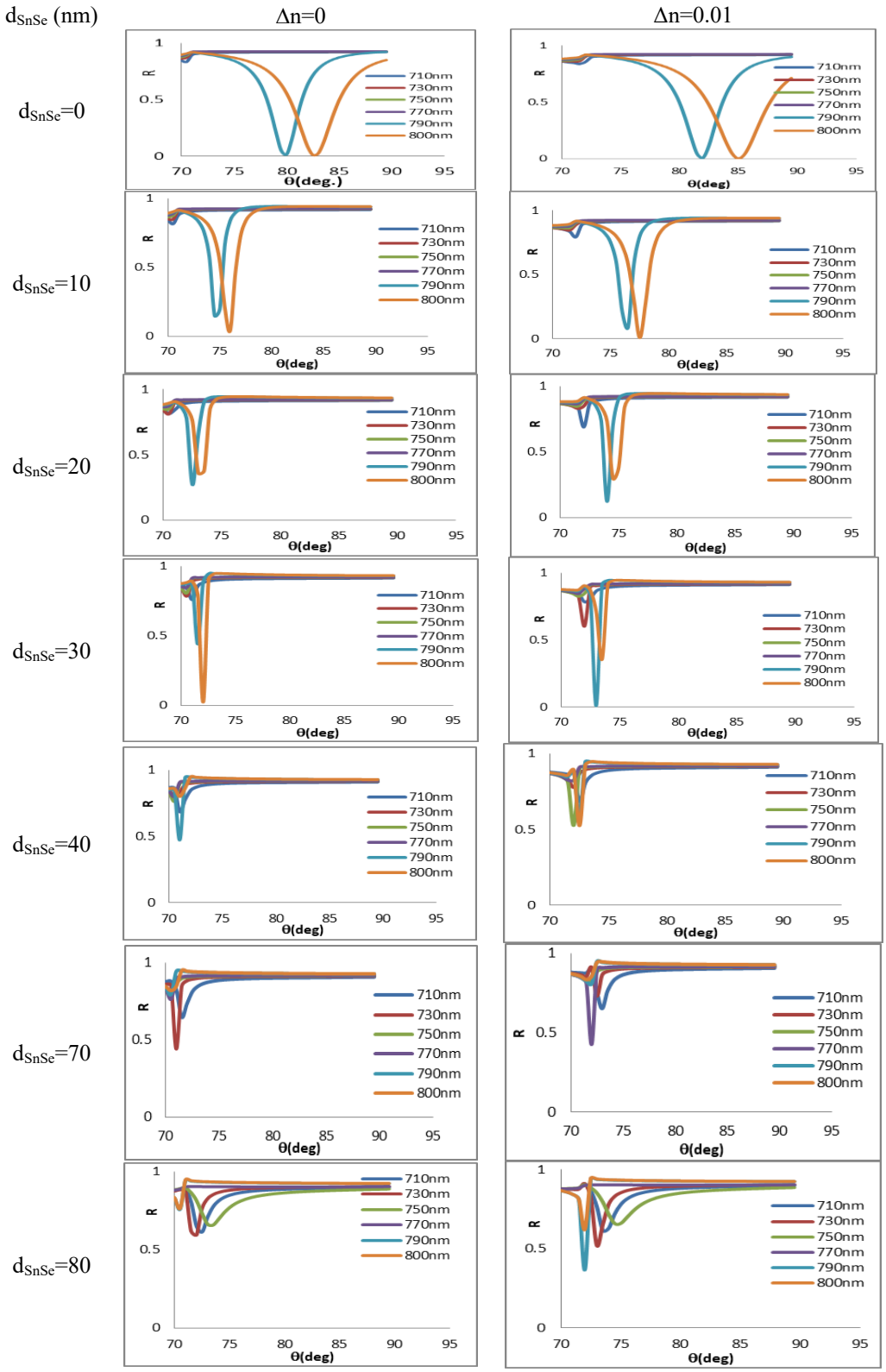

Figure 2: Relation of reflectance and angle (R–θ curve) displaying variations of (Δn) and different range of wavelengths value.

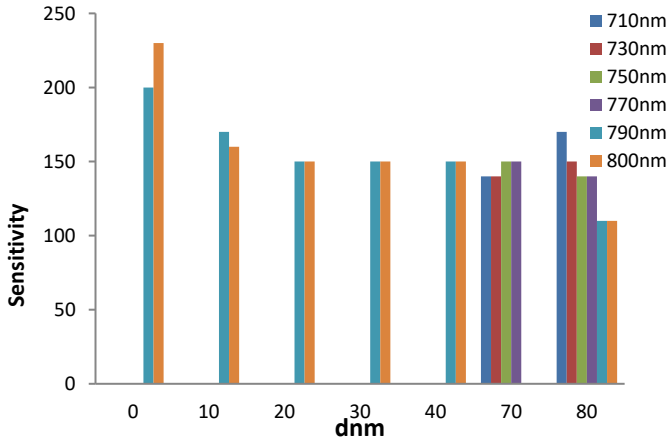

Figure 3: The calculated extent dip and full-width half maximum (FWHM) for different SnSe wavelengths and thicknesses due to refractive indices change.

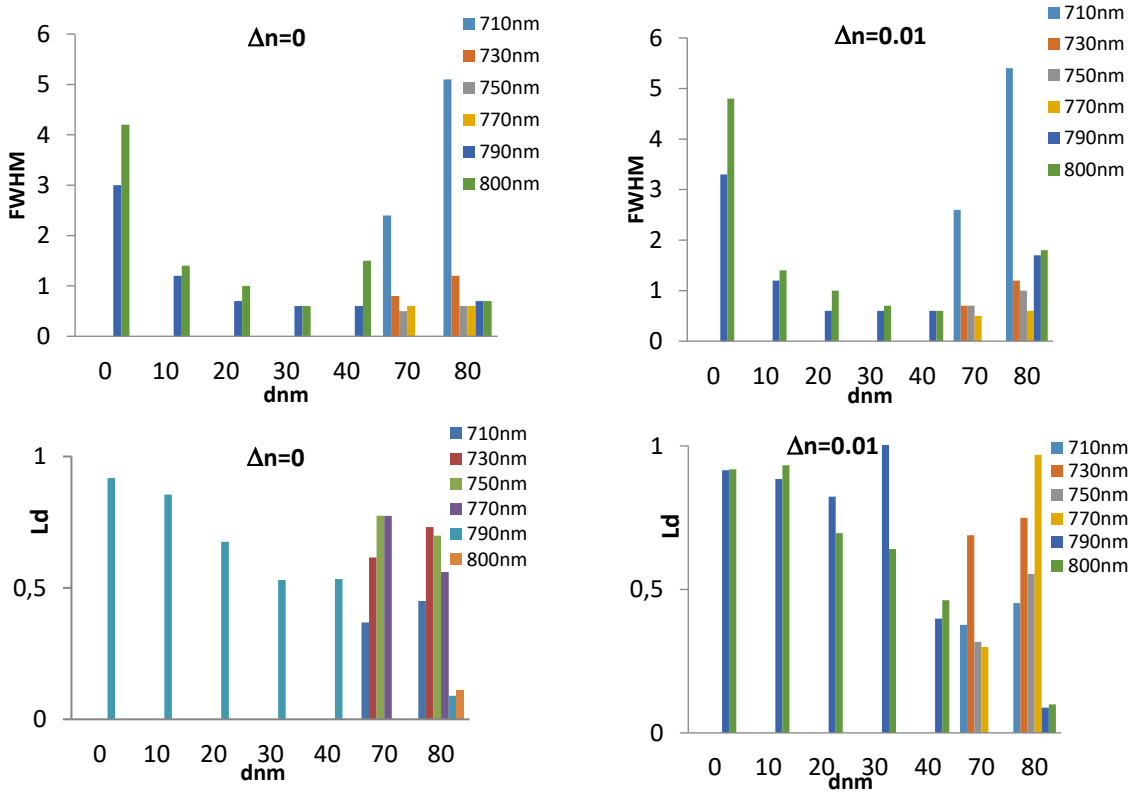

Figure 4: The relationship between the variations in the thickness of SnSe layer and sensitivity at various wavelengths.

The interference from multilayer reflections is not optimal, leading to the absence of a clear SPR dip in the reflectance curve. This phenomenon aligns with multilayer optical systems in which the dielectric layer becomes excessively optically thick, functioning more like a glossy buffer than a field-enhancing layer [24].

In Figure 4 the variations of the SnSe thickness layer affect the sensitivity (S) and the refractive indices of the sensing medium are illustrated. At every thickness level, the relationship between sensitivity and thickness change was weak. Remembering that sensitivity changes as the sensing material's refractive index does is important. The

values illustrated as Δn = 0.01 for different wavelengths of thickness dMoS2 = 40 nm, dSnSe = 0 nm, and dSnSe = 800 nm were S = 230 º /RIU, λ = (790-800) nm, with thicknesses from dSnSe = (0-40) nm. In accordance with [25], its values varied from dSnSe = (70–80) nm for thicknesses to (S = 140–110) º /RIU for thicknesses with rising thicknesses and wavelengths. The relationship between the sensing medium's refractive indices and the sensitivity (S) as a result of variations in the thickness of the SnSe layer illustrates in Figure 4. The correlation between sensitivity and thickness change was poor across all thickness levels. However, it's crucial to keep in mind that sensitivity varies as the refractive index of the sensing material changes. Values (S) for Δn =0.01 at using the wavelength λ=800nm, dMoS2=40nm and dSnSe=0nm, was (S = 230 º /RIU, λ= (790-800) nm where its values ranged between (S = 200-150) º /RIU, for thicknesses from dSnSe = (0- 40) nm. So its values ranged between (S = 140-110) º /RIU for thicknesses from dSnSe = (70- 80) nm with increased thicknesses and wavelengths, which it agrees with [26], [27]. This suggests that the sensitivity high that showed up at Δn low levels is proof of the suggested system's effectiveness. The system's advantage can be utilized as an effective biological sensor within the infrared spectrum at wavelengths of (710, 730, 750, 770, 790, and 800) nm.

The suggested sample for the optical sensor has numerous significant advantages. It is observed that SPR is absent at wavelengths (λ) ranging from (100 to 700) nm, with its onset occurring at 710 nm, where it manifests as an incomplete dip. For the wavelengths of (710, 730, 750, 770, 790) nm, and 800 nm. SPR is observed at every SnSe layer thickness (0–80 nm). The resolution of the sensor was altered with the wavelength, leading to a widening of the reflectance dip. The sensor's accuracy is determined by the dip's shape and its width. At an infrared wavelength of λ= (790-800) nm, the optimal SPR appearance at (dSnSe=30nm) shows that the FWHM for the SPR dip ranges from (0.6° to 0.7°), and the Ld for the SPR dip rises with Δn and wavelengths, measuring between (0.53° and 1°). The maximum dip extent Ld is recorded as (0.96°), while FWHM, the full width half maximum at λ=770 nm is (0.6°), thickness dSnSe = 80nm, at Δn = 0.01. The SPR angle increased slightly with the refractive index of the sensing medium, consistent with [24]. The proposed SPR sensor with sharper shapes achieves a higher sensitivity (S) of 230 °/RIU for Δn =0.01 at the wavelength λ=800 nm, dMoS2=40 nm and dSnSe=0 nm, and in λ= (790-800) nm where its values extended between (S = 200-150) °/RIU, for thicknesses from dSnSe = (0- 40) nm. So its values fluctuated between (S = 140 - 110) °/RIU for thicknesses from dSnSe = (70- 80) nm with increased thicknesses and wavelengths. The relation between the variation in SnSe layer thickness and the refractive index of the sensing medium has a small impact. In this instance, the dip of the R–θ curve shifted because of alterations to the refractive index.

Due to its high refractive index, strong light-matter interaction, and superior charge-transfer capabilities at the metal–dielectric interface, MoS_2 exhibits an improvement in sensitivity. A deeper and sharper SPR dip is produced by these characteristics, which also improve the plasmon–exciton interaction and local electric field. By maintaining strong field confinement without excessive optical loss at an ideal thickness of about 40 nm, MoS_2 enhances overall sensing performance [28].

The MoS_2 layer thickness was fixed at 40 nm because this value provided an optimal balance between plasmonic field confinement and optical loss. At this thickness, MoS_2 enhances the local electric field intensity and improves sensitivity without acting as an excessively thick dielectric buffer that could weaken the SPR. The resonance dip often shifts toward higher incidence angles as MoS_2 thickness increases. This shift is explained by variations in the multilayer structure's optical path length and effective refractive index, which have an impact on the plasmon coupling conditions. The resonance behavior is likewise modulated by varying the thickness of SnSe (0 to 80 nm), however the effect is less pronounced than that of MoS_2. Because of its function in altering the overall dielectric environment next to the metal layer, thicker SnSe layers typically result in a modest further movement of the resonance dip. All thickness choices show the same depth and sharpness of the resonance dip, which suggests strong plasmon excitation and effective sensor operation. The optical constants and plasmonic properties of MoS_2 and SnSe have been added to strengthen the validation of optical parameters used in the simulations [29], [30]. The obtained results confirm that the combination of MoS_2 significantly enhances sensitivity through strong plasmon–exciton coupling, consistent with the recent multilayer study of [31], which demonstrated improved infrared detection performance in MoS_2/graphene-based SPR configurations.

Table 2: Comparison of proposed SPR sensor with other published works.

Reference	Sensor Structure	λ (nm)	Sensitivity (°/RIU)	Notes
This work	BK7 / Ag (50 nm) / SnSe (0–80 nm) / MoS_2 (fixed 40 nm) / Wate	800	230	High IR sensitivity, optimized at dSnSe = 0 nm, dMoS_2 = 40 nm
Ouyang et al., 2016	TMDs / Si nanostructure / Water	633	194	TMDs like MoS_2, WS_2 with Si Nano patterning
[Nisha et al., 2019]	Au / MoS_2 / Ni	633	229	Monitored MoS_2 layers + magnetic substrate
[Lin et al., 2020]	Ag / MoS_2 / Graphene	633	194	Genetic algorithm optimized; visible range
Rahman et al., 2021	SPR fiber / MoS_2	1550	165	MoS_2, Fiber Near-IR fiber-optic configuration
Almawgani et al., 2022	BK7 / BTO (Barium Titanate) / MoS_2	633	160	BTO, MoS_2 Focus on glucose sensing
Singh et al., 2022	Blue Phosphorus / MoS_2 / Si	800	190	MoS_2, BP, Si Hetero structure design
Zeng et al., 2024	Graphene–metal hybrid	650	178	Graphene, Ag Strong enhancement using 2D hybrid
Baidaa K. Hamed et al., 2025	BK7 / Au / SnSe	700	240	Au, SnSe Tunable with SnSe, similar to this study

A steady temperature must be maintained during operation since any large temperature shift could cause refractive index changes, which would impair system performance and result in variations in plasmonic resonance states. But rather than looking at important temperature impacts, this study concentrates on making sure the system runs at ambient temperature.

An evaluation to compare the output results of this study for proposed SPR Sensor with other published works in other references are presented in Table 2. Noticed from the table in this study, the design meets or exceeds the sensitivity of most, particularly in the infrared region (λ = 800 nm), while others are primarily in the visible spectrum. Combining SnSe with MoS_2 allows for tunable dielectric control and improved EM field confinement. To maintain its 2D nanomaterial effect, the MoS_2 layer must be kept at 10 nm.

To compare the simulation results with previously published experimental data, if available, or to clearly indicate the lack of such studies. It is clarified that the simulations in this case represent prospective theoretical studies aimed at identifying the best conditions for obtaining an optimal SPR response before moving to practical implementation. This approach contributes to reducing costs and losses by adopting only cases that have proven successful theoretically, and then implementing and confirming them experimentally.

5 CONCLUSIONS

The proposed Ag/SnSe/MoS_2 multilayer SPR sensor effectively detects small refractive index variations in aqueous media and shows stable performance in the infrared region. A clear SPR response was observed for most SnSe thicknesses (0–80 nm), while it disappeared at 50–60 nm due to non-optimal multilayer interference, where the dielectric layer becomes optically thick and suppresses plasmon excitation.

The optimal configuration achieved a maximum sensitivity of 230 °/RIU at λ = 800 nm, Δn = 0.01, d(MoS_2) = 40 nm, and d(SnSe) = 0 nm, confirming strong field confinement and efficient plasmon coupling. The sensor demonstrated good stability and accuracy under room-temperature conditions; however, maintaining thermal consistency is essential, since temperature fluctuations can alter refractive indices and shift the resonance position.

This method contributes to reducing costs and losses by adopting only cases that have proven successful theoretically, and then applying and confirming them experimentally.

Overall, the designed multilayer structure provides a promising, sensitive, and stable platform for refractive-index sensing and can potentially be extended to practical biosensing applications in aqueous environments.

ACKNOWLEDGMENTS

For its help and assistance with this work, the authors would be like to thank Mustansiriyah University (www.uomustansiriyah.edu.iq) in Baghdad, Iraq.

REFERENCES

[1] J. Homola and M. Piliarik, "Surface plasmon resonance based sensors," Springer, vol. 4, no. 2, pp. 46-47, 2006.

[2] G. Zheng, X. Zou, Y. Chen, L. Xu, and W. Rao, "Fano resonance in graphene-MoS2 heterostructure-based surface plasmon resonance biosensor and its potential applications," Opt. Mater., vol. 66, pp. 171-178, 2017.

[3] A. K. Mishra, S. K. Mishra, and R. K. Verma, "Graphene and beyond graphene MoS2: a new window in surface-plasmon-resonance-based fiber optic sensing," J. Phys. Chem., vol. 120, no. 5, pp. 2893-2900, 2016.

[4] Otto, "Excitation of surface plasma waves in silver by the method of frustrated total reflection," Z. Physik, vol. 216, pp. 398-410, 1968.

[5] E. Kretschmann and H. Raether, "Radiative decay of non-radiative surface plasmons excited by light," Z. Naturforsch., vol. 23A, pp. 2135-2136, 1968.

[6] A. Stefan Maier, Plasmonics: Fundamentals and Applications, Springer Science & Business Media, 2007.

[7] M. Skorobogatiya and A. V. Kabashin, "Photon crystal waveguide-based surface plasmon resonance biosensor," Appl. Phys. Lett., vol. 89, p. 143518, 2006.

[8] M. Saifur Rahman, Md. Shamim Anower, Labid Bin Bashar, and Khaleda Akter Rikta, "Sensitivity analysis of graphene coated surface plasmon resonance biosensors for biosensing applications," Sensing and Bio-Sensing Research, vol. 16, pp. 41-45, 2017, [Online]. Available: http://dx.doi.org/10.1016/j.sbsr.2017.11.001.

[9] A. Nisha, et al., "Sensitivity enhancement of surface plasmon resonance sensor with 2D material covered noble and magnetic material (Ni)," Optical and Quantum Electronics, vol. 51, no. 19, 2019.

[10] Z. Lin, S. Chen, and C. Lin, "Sensitivity improvement of a surface plasmon resonance sensor based on two-dimensional materials hybrid structure in visible region: a theoretical study," Sensors, vol. 20, p. 2445, 2020.

[11] F. J. Kadhum, S. H. Kafi, A. Saeed, A. Al-Zuky, and A. Al-Saleh, "Simulation of surface plasmon resonance (SPR) of silver with titanium oxide as a bi-layer," Biosensor. The Scientific Journal of King Faisal University: Basic and Applied Sciences, vol. 22, no. 2, 2021, [Online]. Available: https://doi.org/10.37575/b/sci/210046.

[12] F. J. Kadhum, A. A. Saeed, M. F. Hadi, A. A. Dawood, and A. H. Al-Saleh, "Theoretical biosensor design for gold-PVA surface plasmon resonance layers," Iraqi Journal of Science, vol. 62, no. 11, pp. 4232-4239, 2021, [Online]. Available: https://doi.org/10.24996/ijs.2021.62.11.

[13] A. M. Alsaad, M. Al-Hmoud, M. W. Marashdeh, M. Aljaafreh, and T. M. Rababah, "Design and modeling of a novel highly sensitive surface plasmon resonance sensor applying tin selenide and graphene for cancer detection," Plasmonics, vol. 19, no. 4, 2023, [Online]. Available: https://doi.org/10.1007/s11468-023-02144-w.

[14] B. K. Hamed, B. H. Hamza, F. J. Kadhum, A. A. Dawood, and A. H. Al-Saleh, "Surface plasmon resonance simulating technology as a bio-sensors," J. Opt., 2025, [Online]. Available: https://doi.org/10.1007/s12596-024-02433-5.

[15] T. Jinguang, J. Li, C. Huifang, W. Yiqin, Y. Ken-Tye, F. Erik, and H. Sailing, "Graphene–bimetal plasmonic platform for ultra-sensitive biosensing," Optics Communications, vol. 410, no. 1, pp. 817-823, 2018.

[16] L. Marques, A. Ricardo, N. Torres, P. João, A. Baptista, M. Marques, and J. Maria, "A new method to analyse the role of surface plasmon polaritons on dielectric-metal interfaces," IEEE Photonics Journal, vol. 14, no. 4, pp. 1-9, 2022, [Online]. Available: https://doi.org/10.1109/JPHOT.2022.3181967.

[17] S. Zeng, D. Baillargeat, H. P. Ho, and K. T. Yong, "Nanomaterials enhanced surface plasmon resonance for biological and chemical sensing applications," Chemical Society Reviews, vol. 43, no. 10, pp. 3426-3452, 2014, [Online]. Available: https://doi.org/10.1039/C3CS60479A.

[18] D. J. B. González, et al., "Plasmonic Au/Co/Au nanosandwiches with enhanced magneto-optical activity," Small, vol. 4, no. 2, pp. 202-205, 2008, [Online]. Available: https://doi.org/10.1002/smll.200700594.

[19] G. Du, et al., "Evidence of localized surface plasmon enhanced magneto-optical effect in nanodisk array," Appl. Phys. Lett., vol. 96, no. 8, p. 081915, 2010, [Online]. Available: https://doi.org/10.1063/1.3334726.

[20] S. Zeng, et al., "Size dependence of Au NP-enhanced surface plasmon resonance based on differential phase measurement," Sensors and Actuators B: Chemical, vol. 176, pp. 1128-1133, 2013, [Online]. Available: https://doi.org/10.1016/j.snb.2012.09.073.

[21] J. Chylek, D. Ciprian, and P. Hlubina, "Optimized film thicknesses for maximum refractive index sensitivity and figure of merit of a bimetallic film surface plasmon resonance sensor," The European Physical Journal Plus, vol. 139, no. 11, 2024, [Online]. Available: https://doi.org/10.1140/epjp/s13360-023-04798-1.

[22] L. Marques, et al., "A new method to determine the response of Kretschmann's structure-based biosensors," IEEE Sensors Journal, vol. 1, pp. 99, 2022, [Online]. Available: https://doi.org/10.1109/JSEN.2022.3207896.

[23] H. Yadgar, et al., "Optimization of surface plasmon resonance (SPR) for gold/air interface by using Kretschmann configuration," Engineering and Technology Journal, vol. 40, no. 10, pp. 1334-1341, 2022.

[24] G. Svitlana, A. Ruslan, and B. Victor Taranenko, "Using metal-multilayer-dielectric structure to increase sensitivity of surface plasmon resonance sensor," Nanoscale Res. Lett., vol. 24, no. 12, p. 295, 2017, [Online]. Available: https://doi.org/10.1186/s11671-017-2073-1

[25] O. Qingling, et al., "Sensitivity enhancement of transition metal dichalcogenides/silicon nanostructure-based surface plasmon resonance biosensor," Scientific Reports, 2016, [Online]. Available: https://doi.org/10.1038/srep28190.

[26] B. Max and W. Emil, Principles of Optics: Electromagnetic Theory of Propagation, Interference and Diffraction of Light, 7th expanded edition, Cambridge University, Margrate Farly & Emil Wolf, 1999.

[27] S. Singh, et al., "Sensitivity enhancement of SPR biosensor employing heterostructure blue phosphorus/MoS2 and silicon layer," Emerging Materials Research, vol. 11, no. 2, pp. 239-250, 2022, [Online]. Available: https://doi.org/10.1680/jemmr.22.00009.

[28] Z. Soraya, K. Alireza, and Z. Naser, "Performance enhancement of surface plasmon resonance biosensors based on noble metals-graphene-WS2 at visible and near-infrared wavelengths," Plasmonics, vol. 15, pp. 309-317, 2020, [Online]. Available: https://doi.org/10.1007/s11468-019-01056-y.

[29] A. Fatma Sayed, A. Hussein Elsayed, and M. Ahmed, "Enhanced angular surface plasmon resonance sensor featuring Ag nanoparticles embedded within a MoS2 hosting medium," Plasmonics, vol. 20, pp. 8167-8183, 2025.

[30] A. Narry, M. Moussa, L. Sungah, and H. Seong, "MoS2–plasmonic hybrid platforms: next generation tools for biological applications," Nanomaterials, vol. 15, no. 2, p. 111, 2025, [Online]. Available: https://doi.org/10.3390/nano15020111.

[31] S. F. Ahmed, M. S. Rahman, and A. T. M. Hossain, "Enhanced performance of a multilayer surface plasmon resonance biosensor incorporating MoS2/graphene hybrid structure for infrared detection," Plasmonics, vol. 20, pp. 8123-8136, 2025, [Online]. Available: https://doi.org/10.1007/s11468-025-03122-3.